Journal of Applied Fluid Mechanics, Vol. 16, No. 12, pp. 2459-2470, 2023.
Available online at www.jafmonline.net, ISSN 1735-3572, EISSN 1735-3645.
https://doi.org/10.47176/jafm.16.12.1890

Vertical and Spanwise Wake Flow Structures of a Single Spire over Smooth Wall Surface in a Wind Tunnel

M. A. Fitriady[1,3], N. A. Rahmat[1,†], and A. F. Mohammad[2]

[1] *Faculty of Mechanical and Automotive Engineering Technology, Universiti Malaysia Pahang (UMP), Malaysia*
[2] *Malaysia-Japan International Institute of Technology, Universiti Teknologi Malaysia (UTM), Malaysia*
[3] *Research Center for Chemistry, Nasional Research and Innovation Agency (BRIN), Indonesia*

†*Corresponding Author Email: izzatulatikha@ump.edu.my*

ABSTRACT

The aerodynamic interaction between the wake flow structure behind a single spire with a smooth wall boundary layer at a long streamwise location was observed in a wind tunnel experiment. The application of a single spire is intended to generate a wake flow similar to the one generated behind a skyscraper. A quarter elliptic wedge spire was used and a long streamwise distance of up to 26 times the spire's height was adopted to ensure the development of the boundary layer and the wake recovery. To grasp how the smooth wall boundary layer interacts with the wake as well as how the wake recovers downstream, vertical and lateral velocity profiles were examined. Despite only one spire being utilized, it was found that the role of the spire as a vortex generator was confirmed the boundary layer height in the with-spire case increased compared to that of the without-spire case. Moreover, the velocity deficit recovery process was observed vertically and streamwise. However, within the boundary layer, the recovery rate in the streamwise direction was lower compared to the above it. This finding indicates that within the boundary, the turbulence generated can sustain the wake caused by the spire, reducing the recovery rate. Based on the current lateral velocity analysis, the final streamwise distance required by the wake to fully recover could not be predicted due to the large velocity deviation of 2.15% at the end of the streamwise distance.

Article History

Received May 5, 2023
Revised August 1, 2023
Accepted August 21, 2023
Available online October 8, 2023

Keywords:

Spire
Wind tunnel experiment
Velocity profile
Velocity deficit
Boundary Layer

1. INTRODUCTION

In an urban area, wind controls the mass and heat transfer which plays a big role in air pollution dispersion. Urban design, building form, and urban density are just a few of the variables that affect the city's wind flow and together they cause various wind environmental conditions (Yang et al., 2020). A highly-urbanized region can be characterized by the presence of high-rise buildings and high building density. Increased building density will disrupt airflows throughout the city, resulting in poor wind environments such as velocity deficit zones caused by the deceleration of airflows (Kubota et al., 2008). A velocity deficit in air flow hinders the heat transfer of a hot surface as well as reduce the mass transfer of air pollutant, hence increasing the temperature in the urban area widely known as the Urban Heat Island (UHI) phenomenon (Mei & Yuan, 2022). This is the critical factor of the UHI effect concerning city planning and development.

Several studies were conducted to investigate the effect of city planning on airflow velocity. Li et al. (2019), who investigated how urban design affected air pollutants dispersion said that the dispersion of air pollutants varied depending on the urban shape and location. Deng et al. (2012), who developed a new urban ventilation model based on the physical and lumped mathematical model, discovered a substantial negative correlation between the urban heat island intensity as well as air pollutant concentration, and the urban ventilation rate by means of wind speed and urban mixing layer height. In addition, a study to examine the flow structure around a 3D model of a traditional Malay house was conducted. It was found that the stagnation point still can be observed based on the model. Hence, an opening was needed in the future design (Rahmat et al., 2023).

Hagishima et al. (2009) investigated the influence of different basic city layouts on three aerodynamic parameters including displacement height (d), the drag coefficient (C_d), and roughness length (Z_o). The roughness

NOMENCLATURE

UHI	Urban Heat Island	U	streamwise velocity
C_d	drag coefficient	U_{ref}	reference velocity
Z_o	roughness length	δ	BLH thickness
d	displacement height	U_n^{WO}	normalized velocities for the WO case
C_p	pressure coefficient	U_n^{WS}	normalized velocities for the WS case
CFD	Computational Fluid Dynamic	ΔU_n	velocity deficit
λ_f	frontal area densities	δ_{ref}	reference BLH thickness
λ_p	plan area index	ΔU_{max}	maximum velocity deficit
WO	without spire case	ΔU_n^{max}	maximum value of velocity deficit
WS	with spire case	ΔU_n^{min}	higher minimum velocity deficit
x	streamwise coordinate distance	$y_{0.5}$	half-wake width
y	spanwise coordinate distance	a	empirical constant
z	vertical coordinate distance		

density was also incorporated as a study variable. Furthermore, Zaki et al. (2011, 2012) expanded the experiment by applying a random set of cubes, which is not covered in the previous study, and generate a prediction equation to explain the relationship between the bulk pressure coefficient (C_p) and the block packing densities. In addition, Mohammad et al. (2018) develop a Computational Fluid Dynamic (CFD) simulation case of flows over vertical random arrays, which is configured based on the frontal area densities (λ_f) variable using the staggered layout to estimate the C_d based on the sheltering of buildings that are parameterized using the normalized individual building's C_p.

Referring to those studies, it was found that, based on the estimated C_d and Z_o, the staggered arrays are more sensitive to the change of the frontal area index (λ_f) and plan area index (λ_p) compared to the square arrays. In addition, the impact of wind direction and the irregularity of building heights on urban aerodynamic parameters vary significantly with λ_p and λ_f which is indicated by the stronger C_d in tall buildings compared to that of short buildings (Hagishima et al., 2009). In the presence of randomness, it was found that, for the $\lambda_p \geq 17\%$, the C_d was greatly affected by the standard deviation of the block height (σ), however, it was independent if λ_p is equal to *7%* (Zaki et al., 2011). In addition, a semi-empirical model of C_d based on C_p is formulated (Mohammad et al., 2018).

On the other hand, Rahmat et al. (2016) propose employing a single-quarter elliptic-wedge spire to mimic the wake flow caused by the skyscraper. This spire is designed to resemble a tall, thin, and solitary building in an urban setting. Furthermore, the study aimed to observe the wake flow structure generated behind a quarter elliptic-wedge spire because wind engineers and climatologists widely utilized a row of these spires as a vortex generator to deepen the atmospheric boundary layer developing in the wind tunnel. Since the velocity deficit is significantly related to the UHI effect, it is very important to observe the wake flow behind a structure to investigate the area affected by the velocity deficit caused by the building (Nagawkar et al., 2014).

Rahmat et al. (2016) performed the wind tunnel experimental work across a fairly short streamwise distance ($x = 1.55S$ and $x = 2.74S$). As a result, it is difficult to observe the velocity recovery rate in the spanwise direction from only 2 streamwise positions. Hence, the total streamwise distance needed by the wake to recover and achieve <1% velocity deviation in the spanwise direction is impossible to be predicted. This is significant for the process of designing a city layout since this distance is equal to the influenced area of the velocity deficit by a skyscraper, hence, the effect of UHI.

Due to the above circumstances, the current study is aimed at observing the aerodynamic interaction of the smooth wall boundary with wake structures behind a single spire layer in a long streamwise distance, up to 26 times the spire's height ($x = 26S$). The vertical and lateral velocity profiles were analyzed to determine the maximum velocity deficits and half-wake width at each height and streamwise position. The rest of this paper is structured as follows; the methodology of the current study is explained in Section 2, followed by Section 3 which presents and discusses the result of the current study and Section 4 which presents the conclusions.

2. METHODOLOGY

2.1 Boundary Layer Wind Tunnel and Spires

A *2.5 m* of streamwise length, open-circuit, and suck-through wind tunnel was utilized to conduct the experiment at Kyushu University's Interdisciplinary Graduate School of Engineering Sciences laboratory. The test section of the wind tunnel is *0.3 m* high and *0.3 m* wide. Due to the inherent impact of the contraction section, the spatial spanwise variation of the mean flow velocity is high especially at just above the bottom of the tunnel ($z \leq 20mm$) as presented in Fig. 1. Therefore, a flat plate was incorporated to generate a new smooth wall background as applied in Rahmat et al. (2018).

Based on Fig. 1, the effect of the flat plate is rather significant near the wall surface. For instance, it can be seen that at $z = 10$ *mm*, the percentage of variation for the case without the flat plate is up to *1.5%*, whereas for the case with the flat plate, the percentage of variation is reduced to about *0.7%*. However, the percentage of the spanwise variation shows a consistently lower percentages trend further downstream for both cases, without flat plate data are mostly higher than the with flat plate data.

This is due to the large spanwise variation of the mean flow caused by the inherent effect at the exit of the

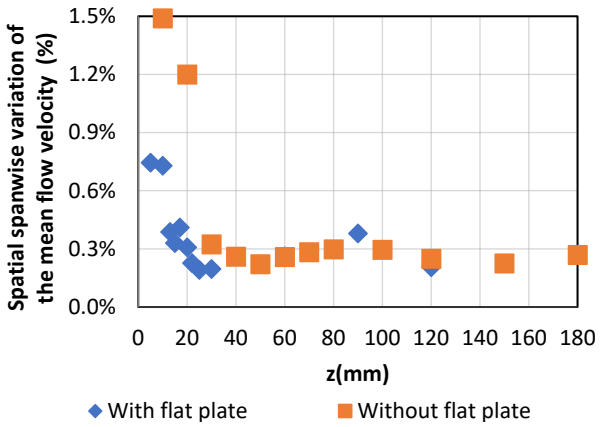

Fig. 1 Percentage of the spatial spanwise variation of the mean flow velocity at various vertical distances from the wall surface for two conditions, with and without the flat plate

contraction part of the tunnel and the fan. Therefore, it is decided to include the flat plate as the new smooth wall surface to reduce the spanwise variation of the mean flow very close to the wall.

Two different settings were incorporated into this experiment. The first setting served as a benchmark or control with no spires (hereafter, the WO case). A single quarter elliptic-wedge spire was used (hereafter, the WS case) for the second set. The spire model has a quarter elliptical form as utilized in the previous study (Counihan, 1969). It measures *0.05 m* in height (*S*), *0.025 m* in length (*0.5S*), and *0.005 m* in width (*0.1S*) while the wedge angle is 5.71°. The spire was positioned 2S from the flat plate's leading edge in the upwind position.

Figure 2 depicts the schematic figure with dimensions of the test section, the quarter elliptic-wedge spire, and the wind tunnel set-up. The axes *x*, *y*, and *z* represent the streamwise, spanwise, and vertical coordinate distances, respectively.

2.2 Measurement Positions and Instrumentations

For both with (WS) and without spire (WO) cases, the streamwise velocity distribution were measured at seven locations in the lateral-vertical planes, ranging from a near-wake of *x = 0.5S*, *S*, *3S*, and *5S* to a far wake of *x = 13S*, *17S*, and *26S*. For each lateral-vertical plane, measurements were conducted at 43 lateral positions and 12 different heights up to *z = 1.2S (0.06 m)*. Detailed measurement conditions are summarized in Table 1.

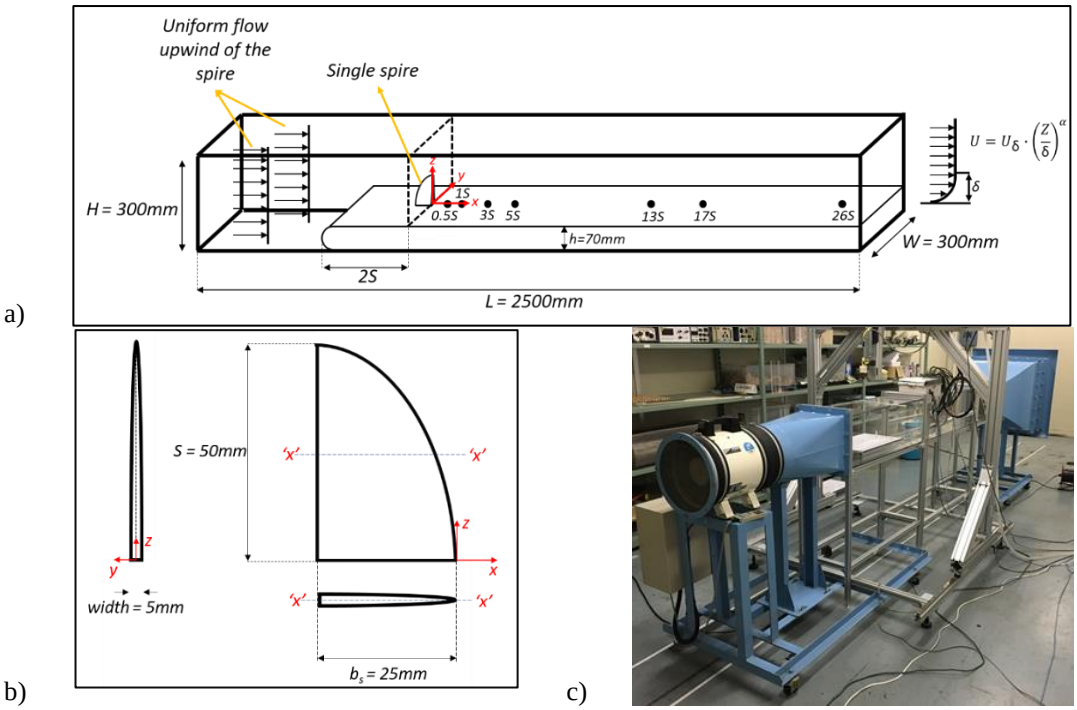

Fig. 2 Schematic figure of a) test section and its measurement points with quarter-elliptic-wedge spire and flat plate; b) installed quarter elliptic-wedge spire and its dimensions; c) the setup of the wind tunnel experiment

Table 1 Measurement condition for both streamwise and vertical distance in the wind tunnel

case	*x*						
	0.5S	*S*	*3S*	*5S*	*13S*	*17S*	*26S*
WO	12 points in vertical direction $0 \le z \le 1.2\ S$ $-1.6S \le y \le -1S$ and $1.6S \le y \le 1S$ at interval *0.01m* $-1S \le y \le -0.4S$ and $1S \le y \le 0.4S$ at interval *0.003m* $-0.4S \le y \le 0.4S$ at interval *0.001m*						
WS							

The streamwise velocity was measured using a single hot-wire anemometer (I-type, Kanomax, 0251R-T5) and a CTA unit (Kanomax, Model 1010). The measurements were performed at 1000 Hz and for 30 s. The data was collected using a data logger (Graphtec, GL900). The stream velocity used for all measurements was 10 ms^{-1}. A pitot tube is then used to calibrate the hot-wire anemometer at least once every 24 hours.

3. RESULT AND DISCUSSION

To compare the velocity profile, the data obtained from the two cases i.e. WO and WS, are analyzed and presented in this section. This section discusses the vertical and lateral velocity profiles in detail.

3.1 Vertical Velocity Profile

Figure 3 presents the vertical velocity profiles at the center of the lateral direction ($y = 0$) for both WO and WS cases. U/U_{ref} is the streamwise velocity (U) normalized by the reference velocity (U_{ref}) that is measured at $y = 0$ and $z = 1.6S$ at each streamwise position.

Based on Fig. 3(a) and (d), due to the wall drag coefficient, the normalized velocity is lowest near the wall at the bottom and increases logarithmically as the vertical distance rises in both the WO and WS cases. Moreover, the highest value of normalized velocity in the WO case was achieved in the near wake region ($0.5S \leq x \leq 5S$) at $z \approx 0.3S$ as presented in Fig. 3(a). This can be caused by the turbulence generation due to the leading edge of the smooth plate. However, this high-value normalized velocity is not observed in the WS case (Fig. 3(d)).

On top of that, the elevation at which the velocity gradient changes is rising as the streamwise distance increases for the WO scenario as presented in Fig. 3(a). It is also observed in the standard deviation graph of the WO case where the value increase as the streamwise distance increase at $z \leq 1S$ as shown in Fig. 3(b). This indicates that the boundary layer is developing along the streamwise direction. However, this development is not observed in the WS case since the elevation at which the velocity gradient changes, is decreasing at the near wake ($0.5S \leq x \leq 6S$) and then increase at the far wake ($13S \leq x \leq 26S$) as observed in Fig. 3(d). It is also shown in the standard deviation graph of the WS case that the value is decreasing at the near wake ($0.5S \leq x \leq 6S$) and then increasing at the far wake ($13S \leq x \leq 26S$) for the vertical distance $z \leq 1S$ as presented in Fig. 3(e).

On the other hand, the skewness profile suggests a different trend. Based on Fig. 3(c) and (f), the height, where the negative peak occurs, is increasing along with the streamwise distance for both WO and WS cases. According to Hagishima et al. (2009), the negative peak of the vertical velocity profile's skewness graph may be

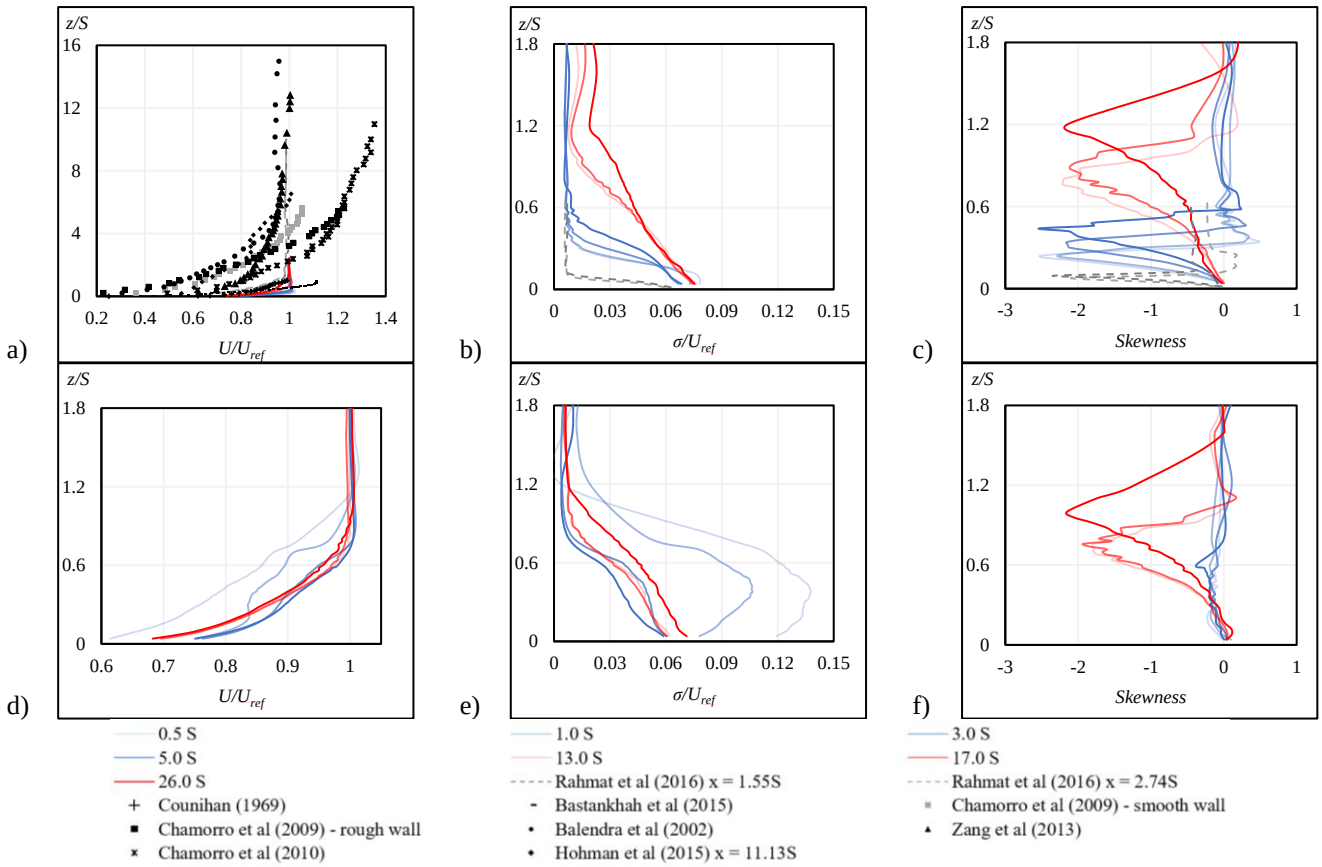

Fig. 3 Normalized vertical velocity profiles at the center point of the wind tunnel for WO case a) mean velocity, b) standard deviation c) skewness; and WS case d) mean velocity e) standard deviation f) skewness. Note: The data of previous studies were included as a comparison (Counihan, 1969;Balendra et al., 2002; Chamorro & Porté-Agel, 2009, 2010; Bastankhah & Porté-Agel, 2015; Zhang et al., 2013; Hohman et al., 2015; Rahmat et al., 2016)

Table 2 Value of the BLH for both the WO and WS case

x / S	WS (δ / S)	WO (δ / S)
0.5	0.2	0.24
1	0.38	0.24
3	0.46	0.34
5	0.6	0.4
13	0.74	0.76
17	0.76	0.88
26	1	1.2

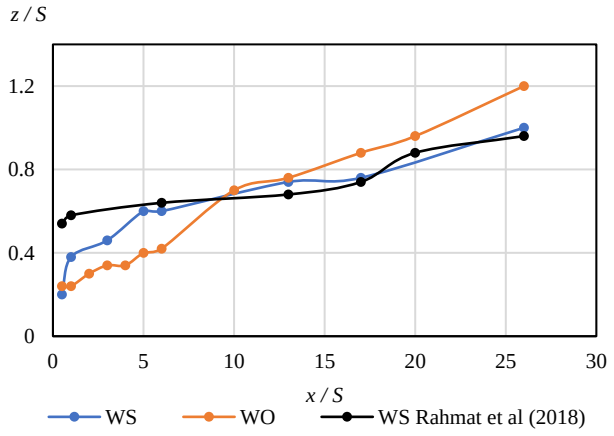

Fig. 4 BLH based on the negative peak of the skewness. Note: BLH generated by Rahmat et al. (2018), which used 5 spires in the experiment, was included as a comparison

used to estimate the boundary layer height (BLH). Therefore, both WO and WS examples show that the BLH is evolving as the streamwise distance grows based on the skewness graph.

Figure 4 presents the BLH obtained from the vertical velocity profile (negative peak of skewness) while the value of the BLH for both WO and WS cases can be seen in Table 2.

3.2 Lateral Velocity Profile

Vertical and Streamwise Distributions of the Lateral Velocity Profile

For WS case, the mean velocity distributions in the lateral-vertical plane at $x = 0.5S$, $1S$, $3S$, $5S$, $13S$, $17S$, and $26S$ are shown in Fig. 5. The contours graph is generated by plotting the streamwise velocities (Un), lateral distance (y), vertical heights (z) in the spreadsheet program and then converted into contour using Avese® application.

Based on Fig. 5, particularly in the near wake ($0.5S \leq x \leq 6S$), the low velocity can be seen near the floor and behind the spire at the center of the lateral direction. As the streamwise distance increased, the wake flow recovered and merge with the expanding smooth wall boundary layer. At $x = 26S$, the wake has merged with the background boundary layer which is in good agreement with Rahmat et al. (2018). As can be observed in the far wake ($13S \leq x \leq 26S$), the boundary layer with velocity deficit laterally heaves with the wavy pattern due to the significant wall shear. These mild lateral heterogeneities in the inflow may be inadvertently produced by the wind tunnel's inlet contraction part, side walls, bottom floors, and ceiling. They progressively become more noticeable as the wall boundary layer develops.

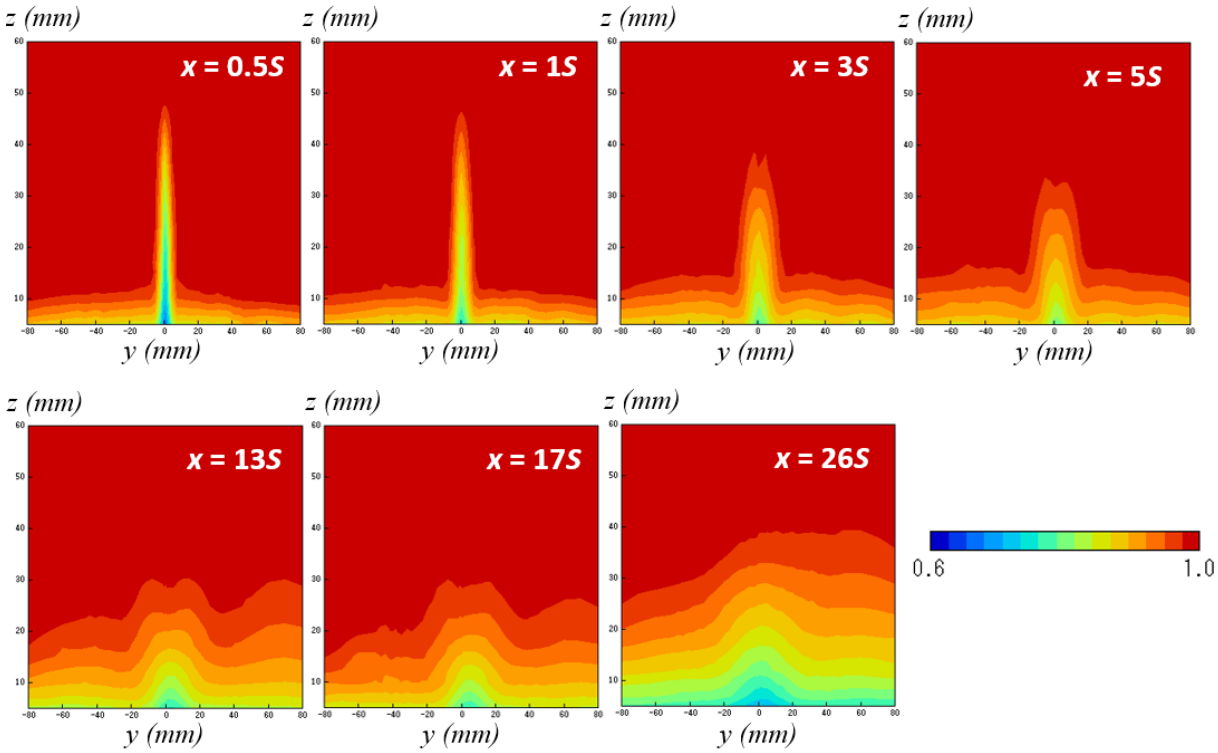

Fig. 5 Contours of streamwise velocity behind a quarter elliptic wedge spire (WS case) at $x = 0.5S$, $1S$, $3S$, $5S$, $13S$, $17S$ and $26S$. The x and y-axis are the spanwise and the vertical distance, respectively

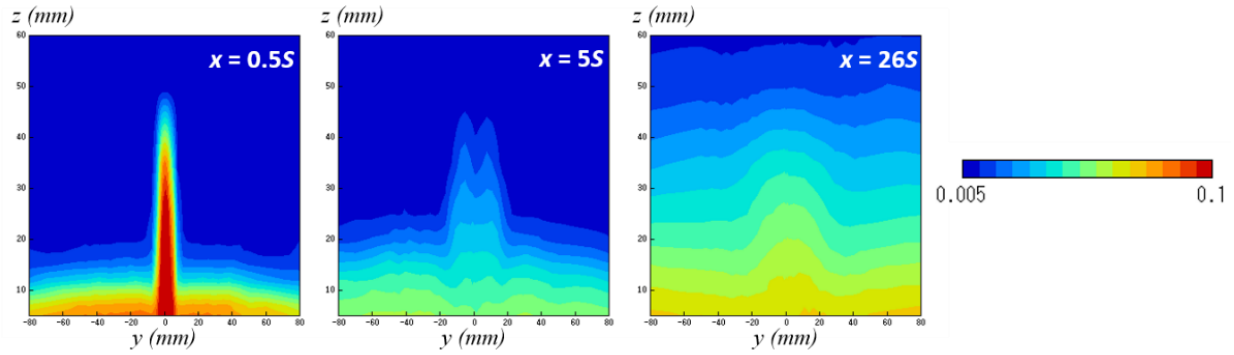

Fig. 6 Contours of the standard deviation of the streamwise velocity behind a quarter elliptic wedge spire (WS case) at *x = 0.5S, 5S* and *26S*

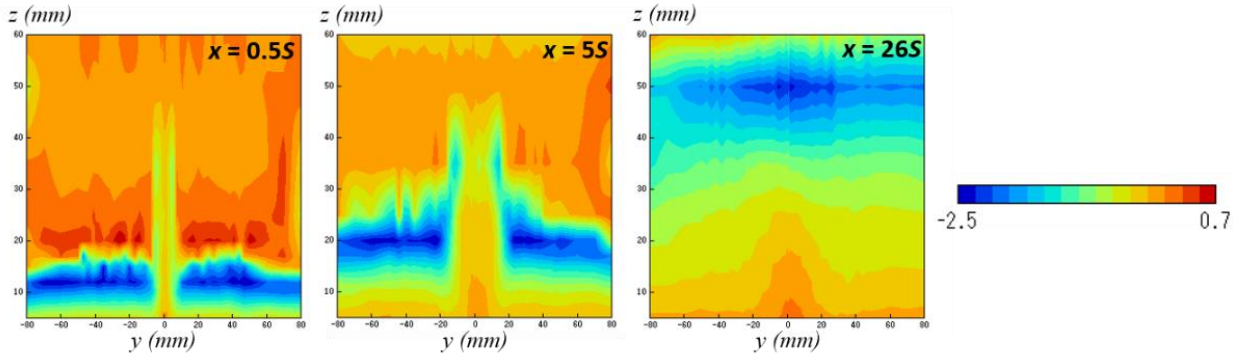

Fig. 7 Contours of skewness of streamwise velocity behind a quarter elliptic wedge spire (WS case) at x = 0.5S, 5S and 26S

Rahmat et al. (2018) reported a similar finding, with low velocity near the floor and behind the spires causing a prominent elliptical peak in the near wake zone. As the streamwise distance rises, the wake flow eventually merges and becomes a deep velocity-deficit layer, as opposed to the layer with a relatively shallow velocity deficit recorded near the center of the lateral direction at $x \geq 20S$.

The streamwise velocity contours of the standard deviation and skewness behind a quarter elliptic wedge spire (WS case) at $x = 0.5S$, $5S$ and $26S$ were presented in Fig. 6 and Fig. 7, respectively. These patterns correspond with the skewness and standard deviation of the velocity (Fig. 3), both of which increase as the location gets closer to the floor.

Within the wall boundary layer, strong upper motion occurs on the sides of the spire. In contrast, weak downward motion occurs behind the spire, which is probably caused by a very slow wind speed due to the spire. Thus, a secondary vortex flow is created owing to these opposite motions. Emerged secondary vortex flow caused a wake flow past the spire persistent downstream because it can supply enough momentum to maintain the wake flow further downstream, hence, hindering the recovery rate.

To observe the wake behind the spire, the lateral velocity profile was plotted in pair of WS and WO cases. Figure 8 shows the velocity distributions in the spanwise direction for several chosen heights at $x = 1S$. The velocity was normalized based on Eq. (1) as follows;

$$U_n(x,y,z) = \frac{U(x,y,z)}{U_{ref}(x,\ y=1.6S,\ z=1.6S)} \quad (1)$$

The reference point is at $y = 1.6S$ and $z = 1.6S$ where the effect of the spire should be minimal.

According to Fig. 8, the negative peak, which indicates the reduced velocity caused by the spire, can be observed at the center of the lateral direction in all vertical distances. Furthermore, at a height of $z = 0.58\delta$ and spanwise distance of $y = \pm 0.2S$, a positive peak was found. However, this positive peak rapidly decreased as the vertical distance rose, as it is not observed in streamwise distance $x \geq 5S$. This prediction is in good agreement with the previous study. Rahmat et al. (2016) also reported a comparable finding where the negative and positive peaks were observed at the height of $z = 0.2\delta$ and 0.5δ. Moreover, the negative peak was reported to be slightly shifted to the negative y direction and the positive peak is absent at the higher position. To deepen the understanding of reduced velocity caused by the spire, a calculation of velocity deficit was conducted.

Spanwise and streamwise variation of velocity deficit

Commonly, velocity deficit was used to characterize a 2D wake in a free shear layer. Based on Rahmat et al. (2016), the velocity deficit can be calculated using the normalized velocity as described in Eq. (2) as follows;

$$\Delta U_n = {U_n}^{WO}{}_{(x,y,z)} - {U_n}^{WS}{}_{(x,y,z)} \quad (2)$$

where ${U_n}^{WO}$ and ${U_n}^{WS}$ are the normalized velocities for both WO and WS cases, respectively.

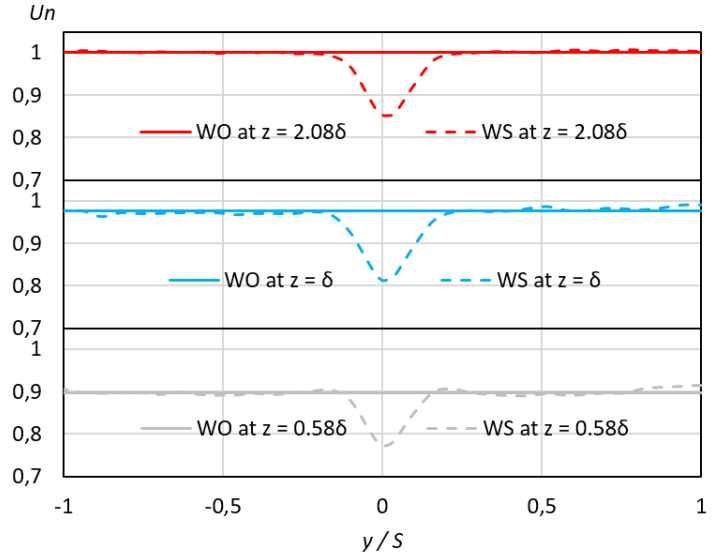

Fig. 8 Velocity distribution in spanwise direction for several chosen heights at *x* = *S*. Note: the dashed line is the WS case while the full line is the WO case. The vertical distance was normalized with the BLH of the WO case (*δ*) based on Table 2

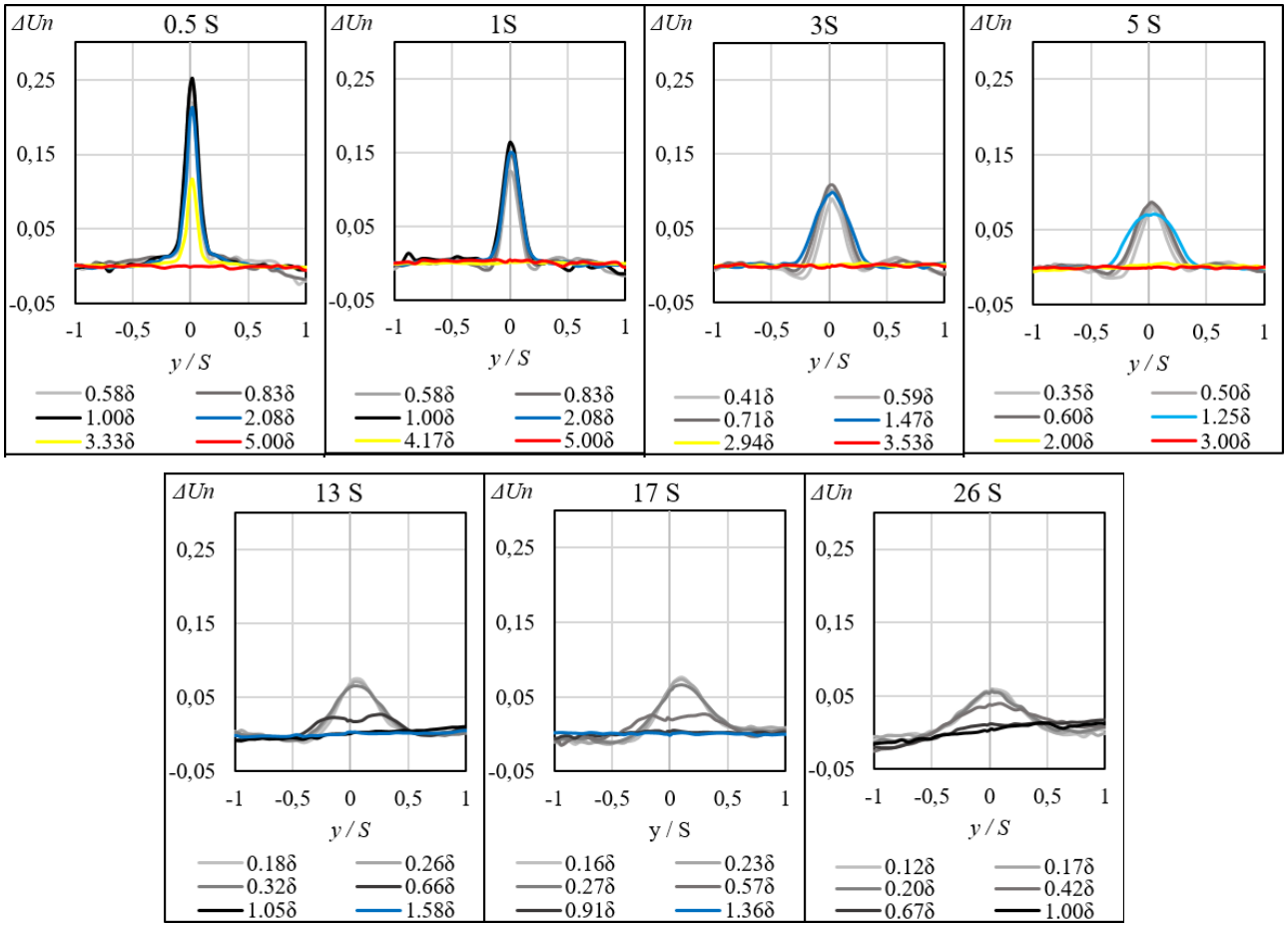

Fig. 9 Spanwise distribution of velocity deficit (ΔU_n) at several vertical distances for all streamwise distances. The vertical distance was normalized with the BLH of the WO case (*δ*) based on Table 2. The grey and blue line indicates within and above the BLH respectively, while the black line is at the BLH. Yellow and red lines indicate the further and furthest above the BLH respectively

Figure 9 presents the velocity deficit ΔU_n of the spanwise distributions at all streamwise distance. To get a detailed spanwise variation of velocity deficit, Fig. 9 for *x* = *1S* is referred to.

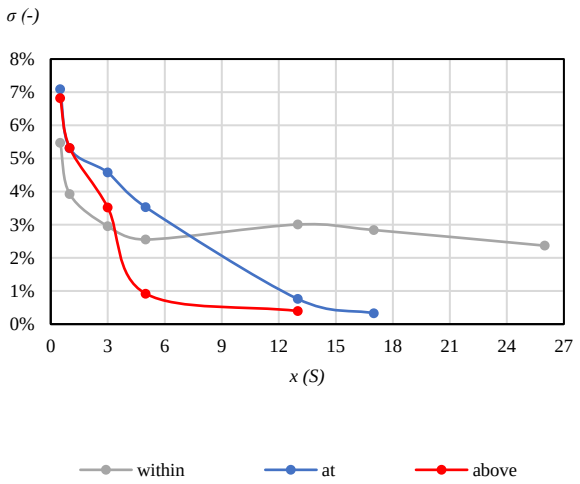

Fig. 10 Spatial relative standard deviation of velocity deficit within, at and above the BLH

Based on Fig. 9 for $x = 1S$, the positive peaks of velocity deficit (ΔU_n) can be observed at the center of the lateral direction ($y = 0$) at all height variables. This peak gradually decreases as the spanwise direction increase in both positive and negative lateral direction. However, the ΔU_n is not completely recovered to zero at the end of the spanwise distance. It is also found that the positive peaks of ΔU_n above the BLH case ($z = 0.5S$) are larger than that within the BLH case ($z = 0.14S$). Moreover, there are two negative peaks observed in the ΔU_n graph within the BLH at approximately $y = \pm 0.2S$ that gradually recovered as the spanwise distance increased in both lateral directions. However, these negative peaks are only observed at $x = 1S$, and $3S$, while in $x = 5S$, the negative peak can only be observed at the negative side of the spanwise direction ($y = -0.3S$).

The whole of Fig. 9 is referred to have a complete observation of the streamwise variation in velocity deficit. The peak of the velocity deficit is seen in the figure to be diminishing as the streamwise distance rises. This phenomenon is often referred to as the wake flow recovery process along the streamwise direction. In the present investigation, the wake flow recovery process took place within, at, and above the BLH. Additionally, the spatial relative standard deviation of velocity deficit may be used to corroborate this recovery as can be seen in Eq. (3).

$$\sigma_{(\Delta U_n)} = \sqrt{\sum \frac{\left(\Delta U_{n(x,y,z)} - \mu_{(x,z)}\right)^2}{n}} \quad (3)$$

Where μ is the lateral average of velocity deficit within, at, and above BLH for each streamwise distance. While n is the total sampling point in the lateral direction. Figure 10 presents the spatial relative standard deviation of velocity deficit within, at and above the BLH.

Based on Fig. 10, it can be stated that the spatial relative standard deviation decreases along with the streamwise distance, which represents the recovery process of velocity deficit occurring in the streamwise direction. To compare the velocity deficit recovery process within, at, and above the BLH, an observation of the rate of recovery was done based on the decrease of the spatial relative standard deviation of lateral velocity in pair of adjacent streamwise distances. The recovery rate was calculated using Eq. (4) for each point in particular.

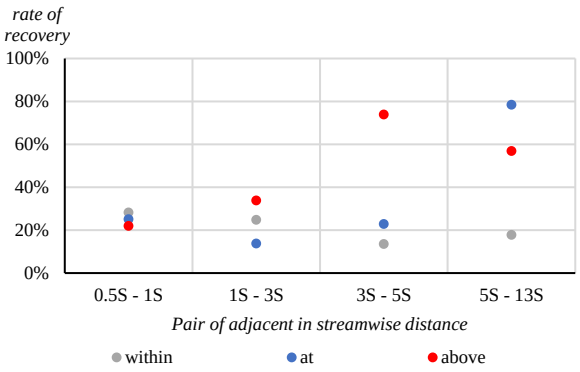

Fig. 11 Recovery rate of a pair of adjacent in the streamwise distance within and above BLH

$$recovery\ rate\ (\%) = \frac{\left(\sigma_{(\Delta U_n)_x} - \sigma_{(\Delta U_n)_{x+1}}\right)}{\sigma_{(\Delta U_n)_x}} \cdot 100\% \quad (4)$$

The rate of recovery of a pair of adjacent streamwise distances is presented in Fig. 11.

Based on Fig. 11, the recovery rate of velocity deficit above the boundary is larger than within the BLH at all streamwise directions in the near wake region, except for pair $0.5S \leq x \leq 1S$ is observed. This might be caused by the lower turbulence above the BLH compared to within the BLH. In other words, turbulence generated within the BLH can sustain the wake flow and reduce the recovery rate along the streamwise direction. The calculation is only for the near wake because in the far wake ($x \geq 13S$) the wake flow above the BLH is already recovered. Hence, the comparison within and above BLH cannot be conducted in the far wake ($x \geq 13S$) region.

This phenomenon is in good agreement with Rahmat et al. (2016) and Ikegaya et al. (2020) who have studied the wake-sustaining mechanism within the BLH in more detail. The updraft, occurring at the wake's center, causes the wake, which is generated within the boundary layer, to sustain more than that observed above the boundary. (Ikegaya et al., 2020).

To observe the sustaining effect of the boundary layer, a maximum velocity deficit (ΔU_{max}) was calculated based on Eq. (5) as follows:

$$\Delta U_{max} = \Delta U_n{}^{max} - \Delta U_n{}^{min} \quad (5)$$

where ΔU_n^{max} is the maximum value of velocity deficit, while $\Delta U_n^{min}$is the higher minimum velocity deficit created by the curve based on Fig. 9.

Figure 12 presents the vertical distribution of ΔU_{max} at near and far wake regions. According to Fig. 12, the sustaining impact of the boundary layer is seen in the near wake. The ΔU_{max} increases along with the vertical distance, creating a turning point slightly above the BLH, and then decreases as the vertical distance continues to increase. This phenomenon reveals the boundary layer's ability to sustain the velocity deficit against the vertical recovery process. However, above the BLH, where turbulence is low, the boundary layer's sustaining

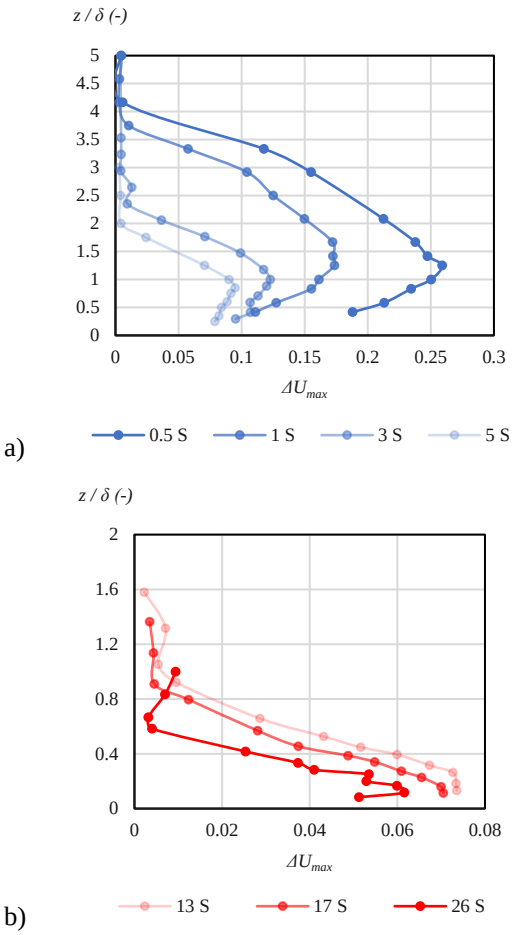

Fig. 12 Vertical distribution of maximum velocity deficit (ΔU_{max}) at a) near wake region and b) far wake region

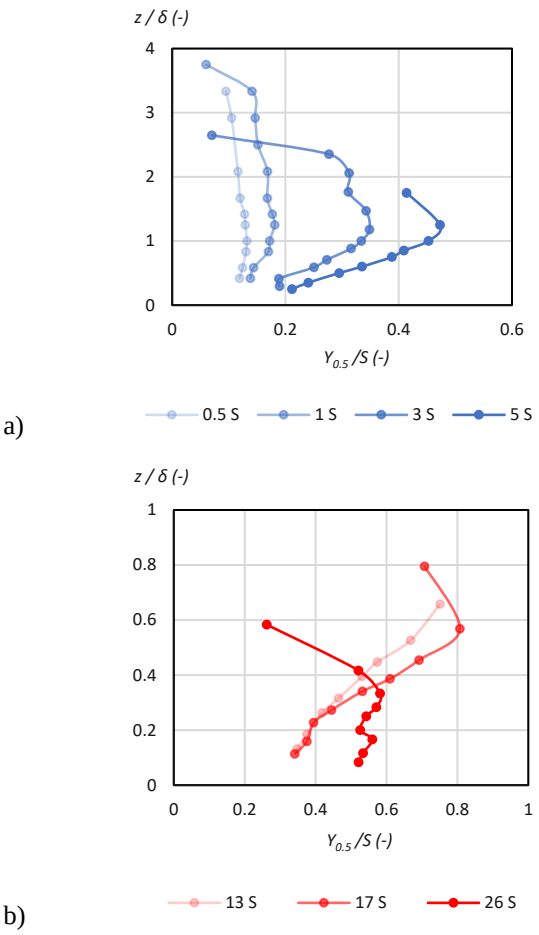

Fig. 13 Vertical distribution of half-wake width at a) near and b) far wake region

influence is absent; hence, the ΔU_{max} begins to recover along with the vertical distance. Although the recovery rate within the BLH region has been reduced, the recovery process is still ongoing since the ΔU_{max} also decreases along the streamwise direction. On the contrary, for the far wake, the ΔU_{max} decrease along with the vertical distance even within the BLH region. The wake flow might be too weak to be sustained by the boundary layer due to the effect of the recovery process along with the streamwise distance at the near wake region.

Vertical Distribution Of Half-Wake Width

The total streamwise distance required by the wake to be fully recovered, hereafter the wake recovery distance, can be predicted based on the half-wake width ($y_{0.5}$) which can be determined as the distance between two interception points created by a horizontal line placed at the half-wake based on Fig. 9. The half-wake is calculated using Eq. (6).

$$half\ wake = \frac{1}{2} \cdot (\Delta U_n^{max} - \Delta U_n^{min}) \quad (6)$$

where $\Delta U_n{}^{max}$ is the maximum and $\Delta U_n{}^{min}$ is the minimum value of ΔU_n in lateral measurement lines respectively. Figure 13 presents the vertical distribution of half-wake width at several streamwise distances of the current study.

Based on Fig. 13, for both near and far wake regions, the half-wake width ($y_{0.5}$) decreases as the vertical distance increase creating a turning point around BLH then increase along with the vertical distance and increase along with the streamwise distance. On top of that, wake recovery distance can be determined from $y_{0.5}$. Referring to Fig. 13, the wake flow above the BLH is recovered at $x = 13S$, while within the BLH, it is sustained down to the end of the streamwise distance of $x = 26S$. Hence, the wake recovery distance cannot be predicted based on the current study which should be a good topic for future research.

3.3 Wake flow and Gradient Diffusion Model Relation

Generally, the deficit of the velocity caused by a 2D obstruction in a free shear flow can be represented by the general function of the gradient-diffusion model (Schlichting, H., Gersten, 2000) which is presented in Eq. (7).

$$g\left(\frac{y}{y_{0.5}}\right) = exp\left(-a \cdot \left(\frac{y}{y_{0.5}}\right)^2\right) \quad (7)$$

where a and $y_{0.5}$ is an empirical constant and the half-wake width value, respectively. The calculations and plot fittings were conducted to determine the a for each streamwise distance that is presented in Table 3. The data from Rahmat et al (2016) was included as a comparison.

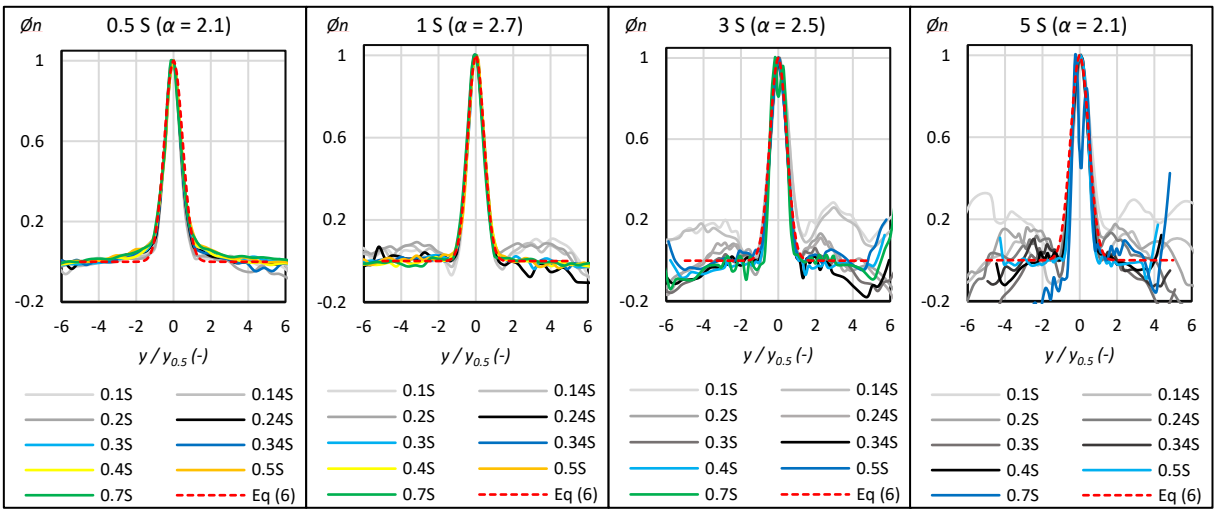

Fig. 14 Comparison of the spanwise distribution of the velocity deficit derived from the wake and that derived from Eq. (7). Note: the grey and the black lines indicate within and at BLH, respectively. While yellow, blue and green line indicates above BLH

Table 3 Empirical constant of general function based on the gradient-diffusion model

	Current study	Rahmat et al. (2016)
x	*α*	*α*
0.5 S	2.17	
1 S	2.66	
2.74 S	-	2.76
3 S	2.76	
5 S	2.11	

Since the velocity deficit has a different baseline, it is normalized to be compared with the gradient-diffusion model. The normalization was calculated using Eq. (8).

$$\emptyset_n = \frac{\left(\Delta U_n - \Delta U_n{}^{min}\right)}{\left(\Delta U_n{}^{max} - \Delta U_n{}^{min}\right)} \quad (8)$$

Figure 14 presents the comparison of the spanwise distribution of the velocity deficit derived from the wake and the one derived from Eq. (7). The *x*-axis is the normalized spanwise distance which is defined as $y.(y_{0.5})^{-1}$. The grey and blue line indicates *within* and *above* the BLH respectively, while the black line is *at* the BLH. Yellow and green lines indicate the further and furthest above the BLH, respectively. All calculations and equations were based on Rahmat et al. (2016).

Based on Fig. 14, the spanwise distributions above the BLH region show a better similarity with the gradient diffusion model compared to that within the BLH. The profile within the BLH shows a significant discrepancy with the gradient diffusion model, especially on $-1.3 \geq (y/y_{0.5}) \geq 1.3$. Hence, the flow structure above the BLH may thus be described as a conventional 2D wake flow of a bluff body in a free stream. However, the similarity is good only for the near wake region up to $x = 3S$ in the streamwise direction. At a distance further than $x = 3S$, the similarity will be decreased significantly.

4. CONCLUSION

A wind tunnel experimental work has been conducted to examine the smooth wall boundary layer interaction with wake structure behind a single spire. Based on the vertical velocity profile, it can be concluded that the BLH is developed in the WS case compared with the one in the WO case, especially at the near wake. It can be assumed that the role of spires as vortex generators to increase the depth of the boundary layer is confirmed.

In addition, from the lateral velocity profile, it can be stated that the velocity deficit recovery process is observed both in vertical and streamwise directions. However, the rate of recovery is lower within the BLH compared to the above BLH due to the high turbulence region. The turbulence generated within the BLH can sustain the wake flow and reduce the recovery rate in the streamwise direction.

Additionally, from the half-wake width analysis, it was found that the wake flow persisted down to the end of the streamwise distance at $x = 26S$ inside the BLH while needing a distance of $x = 13S$ to recover above BLH. Due to the insufficient length of the wind tunnel test section, it is impossible to anticipate wake recovery distance. This presents an excellent chance to explore it using a different technique, such as CFD.

Lastly, following to the relation between the wake flow and gradient diffusion model, it can be concluded that the flow structure above boundary corresponds well with a typical 2D wake of a bluff body in a free stream. However, this is applied only for the near wake region up to $x = 3S$ in the streamwise direction. At a distance further than $x = 3S$, the similarity will decrease significantly.

ACKNOWLEDGEMENTS

The authors gratefully acknowledge the research grant and financial support provided by the Ministry of Higher Education, MOHE (under the FRGS grant number:

FRGS/1/2019/TK07/UMP/02/7 (RDU1901208) and Universiti Malaysia Pahang, UMP (under UMP grant number: RDU190375) also the MRS scholarship.

CONFLICT OF INTEREST

The author stated that there are no conflicts of interest to disclose.

AUTHORS CONTRIBUTION

The wind tunnel experiment was done by Dr. Nurizzatul Atikha Rahmat as a continuation of work from her previous research study. The literature search and the first draft were done by Muhammad Arifuddin Fitriady. Dr. Nurizzatul Atikha Rahmat, as well as Dr. Ahmad Faiz Mohammad, also critically revised the work. All authors have read and approved the final manuscript.

REFERENCES

Balendra, T., Shah, D. A., Tey, K. L., & Kong, S. K. (2002). Evaluation of flow characteristics in the NUS-HDB wind tunnel. *Journal of Wind Engineering and Industrial Aerodynamics*, 90(6), 675–688. https://doi.org/10.1016/S0167-6105(01)00223-9

Bastankhah, M., & Porté-Agel, F. (2015). A wind-tunnel investigation of wind-turbine wakes in yawed conditions. *Journal of Physics: Conference Series*, 625(1). https://doi.org/10.1088/1742-6596/625/1/012014

Chamorro, L. P., & Porté-Agel, F. (2009). A wind-tunnel investigation of wind-turbine wakes: Boundary-Layer turbulence effects. *Boundary-Layer Meteorology*, 132(1), 129–149. https://doi.org/10.1007/s10546-009-9380-8

Chamorro, L. P., & Porté-Agel, F. (2010). Effects of Thermal stability and incoming boundary-layer flow characteristics on wind-turbine wakes: A wind-tunnel study. *Boundary-Layer Meteorology*, 136(3), 515–533. https://doi.org/10.1007/s10546-010-9512-1

Counihan, J. (1969). An improved method of simulating an atmospheric boundary layer in a wind tunnel. *Atmospheric Environment*, 3(2), 197–214. https://doi.org/10.1016/0004-6981(69)90008-0

Deng, Q., He, G., Lu, C., & Liu, W. (2012). Urban ventilation-A new concept and lumped model. *International Journal of Ventilation*, 11(2), 131–140. https://doi.org/10.1080/14733315.2012.11683976

Hagishima, A., Tanimoto, J., Nagayama, K., & Meno, S. (2009). Aerodynamic parameters of regular arrays of rectangular blocks with various geometries. *Boundary-Layer Meteorology*, 132(2), 315–337. https://doi.org/10.1007/s10546-009-9403-5

Hohman, T. C., Van Buren, T., Martinelli, L., & Smits, A. J. (2015). Generating an artificially thickened boundary layer to simulate the neutral atmospheric boundary layer. *Journal of Wind Engineering and Industrial Aerodynamics*, 145, 1–16. https://doi.org/10.1016/j.jweia.2015.05.012

Ikegaya, N., Morishige, S., Matsukura, Y., Onishi, N., & Hagishima, A. (2020). Experimental study on the interaction between turbulent boundary layer and wake behind various types of two-dimensional cylinders. *Journal of Wind Engineering and Industrial Aerodynamics*, 204, 104250. https://doi.org/10.1016/j.jweia.2020.104250

Kubota, T., Miura, M., Tominaga, Y., & Mochida, A. (2008). Wind tunnel tests on the relationship between building density and pedestrian-level wind velocity: Development of guidelines for realizing acceptable wind environment in residential neighborhoods. *Building and Environment*, 43(10), 1699–1708. https://doi.org/10.1016/j.buildenv.2007.10.015

Li, C., Wang, Z., Li, B., Peng, Z. R., & Fu, Q. (2019). Investigating the relationship between air pollution variation and urban form. *Building and Environment*, 147, 559–568. https://doi.org/10.1016/j.buildenv.2018.06.038

Mei, S. J., & Yuan, C. (2022). Urban buoyancy-driven air flow and modelling method: A critical review. *Building and Environment*, 210, 108708. https://doi.org/10.1016/j.buildenv.2021.108708

Mohammad, A. F., Zaki, S. A., Ikegaya, N., Hagishima, A., & Ali, M. S. M. (2018). A new semi-empirical model for estimating the drag coefficient of the vertical random staggered arrays using LES. *Journal of Wind Engineering and Industrial Aerodynamics*, 180, 191–200. https://doi.org/10.1016/j.jweia.2018.08.003

Nagawkar, J., Ghosh, S., Kataria, R., Nashit, A., & Deora, A. (2014). Effect of sky scrapers on natural ventilation patterns and human comfort index in low-risebuildings - a CFD analysis over central Mumbai. *ARPN Journal of Engineering and Applied Sciences*, 9(3), 293–295. https://citeseerx.ist.psu.edu/viewdoc/download?doi=10.1.1.1061.2403&rep=rep1&type=pdf

Rahmat, N. A., Hagishima, A., & Ikegaya, N. (2016). An experimental study on aerodynamic interaction between a boundary layer generated by a smooth and rough wall and a wake behind a spire. *Engineering Sciences Reports, Kyushu University*, 37(2), 19–26. https://api.lib.kyushu-u.ac.jp/opac_download_md/1560669/3724.pdf

Rahmat, N. A., Hagishima, A., Ikegaya, N., & Tanimoto, J. (2018). Experimental study on effect of spires on the lateral nonuniformity of mean flow in a wind tunnel. *Evergreen*, 5(1), 1–15. https://doi.org/10.5109/1929670

Rahmat, N. A., Haji Abdullah, K. K., & Khairunizam, K. A. (2023). *Natural ventilation in traditional malay house: a study of flow pattern by an enhanced smoke*

wire technique. Lecture Notes in Energy https://doi.org/10.1007/978-981-19-6688-0_18

Schlichting, H., & Gersten, K. (2000). *Boundary layer theory* (8th ed.). Springer.

Yang, J., Shi, B., Shi, Y., Marvin, S., Zheng, Y., & Xia, G. (2020). Air pollution dispersal in high density urban areas: Research on the triadic relation of wind, air pollution, and urban form. *Sustainable Cities and Society*, 54, 101941. https://doi.org/10.1016/j.scs.2019.101941

Zaki, S. A., Hagishima, A., & Tanimoto, J. (2012). Experimental study of wind-induced ventilation in urban building of cube arrays with various layouts. *Journal of Wind Engineering and Industrial Aerodynamics*, 103, 31–40. https://doi.org/10.1016/j.jweia.2012.02.008

Zaki, S. A., Hagishima, A., Tanimoto, J., & Ikegaya, N. (2011). Aerodynamic parameters of urban building arrays with random geometries. *Boundary-Layer Meteorology*, 138(1), 99–120. https://doi.org/10.1007/s10546-010-9551-7

Zhang, W., Markfort, C. D., & Porté-Agel, F. (2013). Wind-Turbine wakes in a convective boundary layer: A wind-tunnel study. *Boundary-Layer Meteorology*, 146(2), 161–179. https://doi.org/10.1007/s10546-012-9751-4